Journal of Materials Chemistry A

REVIEW

View Article Online
View Journal | View Issue

Cite this: J. Mater. Chem. A, 2018, 6, 12932

The recent progress of nitrogen-doped carbon nanomaterials for electrochemical batteries

Jingxia Wu,† Zhiyong Pan,† Ye Zhang, Bingjie Wang* and Huisheng Peng *

Carbon nanomaterials have been widely explored for use as electrode materials for the fabrication of electrochemical batteries. Nitrogen doping represents a general and effective method in further improving the physical and chemical properties of carbon nanomaterials to enhance the energy storage capabilities of the resulting batteries. In this review paper, the recent advances in the synthesis and property of nitrogen-doped carbon nanomaterials including carbon nanotubes, graphene, porous carbon, and carbon nanofibers are highlighted first. The use of nitrogen-doped carbon nanomaterials in various electrochemical batteries such as lithium ion batteries, lithium–sulfur batteries, metal–air (oxygen) batteries and sodium ion batteries is then discussed with a focus on their electrochemical properties. The remaining challenges and the possible direction for the use of nitrogen-doped carbon nanomaterials for electrochemical batteries are finally described to provide some useful clues for the future developments of this promising field.

Received 30th April 2018
Accepted 13th June 2018

DOI: 10.1039/c8ta03968b

rsc.li/materials-a

1. Introduction

The search for clean energy sources to alleviate the greenhouse effect as well as to create superior energy storage devices for electronics has boosted the development of various energy storage devices. Batteries, including lithium ion batteries (LIBs), lithium–sulfur batteries, metal–air (oxygen) batteries and sodium ion batteries (SIBs), have been focused on in recent research because of their relatively high energy densities. For example, lithium–sulfur and lithium–oxygen batteries have high theoretical specific capacities up to 1675 mA h g^{-1} and 3860 mA h g^{-1}, respectively.[1] However, the full utilization of the high specific capacity remains challenging and requires researchers to find and explore appropriate electrode materials.

Compared with metallic compounds, which have been widely used as electrode materials, carbon nanomaterials simultaneously display high electrical conductivities, high specific surface areas and good stabilities with little volume expansion during the charge–discharge process.[2–5] The high electrical conductivity facilitates charge transfer and the high specific surface area provides channels for electrolyte and oxygen diffusion. Porous structures with high surface areas enable rapid electrolyte diffusions and charge transfers,[6] which are beneficial for fast charging and discharging. The porous structure may accommodate the volume change of active materials such as silicon (Si) and sulfur (S). However, higher surface areas also lead to higher electrolyte consumptions and more solid electrolyte interfaces. Therefore, a balance needs to be found for the porous electrode materials. However, the poor electrochemical activity, as well as the low theoretical capacity of carbon have limited its application. The chemical properties of carbon nanomaterials can be varied by introducing chemical dopants such as phosphorus, boron and nitrogen (N). The incorporation of heteroatoms can significantly change the nanostructure and electrochemical performance of carbon nanomaterials.

The N-doping strategy represents an effective method in adjusting the physical and chemical properties of carbon nanomaterials because of the following reasons. Firstly, N-doping provides a higher electrochemical activity, and because of the two lone pair electrons, the nitrogen atom is more electronegative than the carbon atom. Thus, the electron density of nitrogen becomes higher (leading to stronger interactions with positive particles), whereas the electron density of the adjacent carbon becomes lower which gives stronger interactions with negative particles. Secondly, N-doping can increase the electrical conductivity of carbon nanomaterials especially with N-doped carbon nanotubes (CNTs) and graphene.[7,8] For example, the electrical conductivity of the N-CNT film reached 410 S cm^{-1}, compared with 200 S cm^{-1} for the bare CNT film.[7] The lone pair electrons in nitrogen and π electrons in CNT and graphene form p–π conjugations which increase the density of the current carrier. Generally, the conductivity of N-doped carbon nanomaterials was verified to be anything from several to hundreds of S cm^{-1} depending on the different carbon materials and synthetic methods used. For example, N-doped carbon nanofibers (CNFs) showed a conductivity of

State Key Laboratory of Molecular Engineering of Polymers, Department of Macromolecular Science, Laboratory of Advanced Materials, Fudan University, Shanghai 200438, China. E-mail: wangbingjie@fudan.edu.cn; penghs@fudan.edu.cn
† These authors contributed equally to this work.

4.9 S cm^{-1},[9] whereas N-doped graphene demonstrated a conductivity as high as 270 S cm^{-1}.[10] Thirdly, a lot of defects are produced after N-doping, and the resulting defects can provide channels for ion and electrolyte diffusion, which are important in batteries.[11]

In this review article, the recent progress in the synthesis of N-doped carbon nanomaterials such as CNTs, graphene, porous carbon, CNFs and others is reviewed, focusing on two different strategies: *in situ* doping and post-treatment. Similar to the carbon materials, N-doped carbon nanomaterials have been widely used as electrodes, conductive additive and electrode substrates in electrochemical batteries. The use of N-doped carbon in a variety of batteries, including LIBs, lithium–sulfur batteries, metal–air (oxygen) batteries and SIBs is then highlighted. Finally, the remaining challenges are discussed to guide future studies.

2. Synthesis of N-doped carbon nanomaterials

There are various synthetic strategies for N-doped carbon nanomaterials, and they are divided into two main categories: *in situ* doping and post-treatment. For the *in situ* doping process, the precursors with nitrogen and carbon atoms were used to synthesize N-doped carbon nanomaterials.[11–13] For the post-treatment strategy, carbon nanomaterials were modified in the presence of various nitrogen sources, and the nitrogen atoms replaced certain carbon atoms.[8,14] The previously described strategies have their advantages and disadvantages. The *in situ* doping method offers uniform distributions of nitrogen atoms with a well maintained structure, whereas the post-treatment strategy may destroy the structure of the carbon precursors, such as the pore size and morphology. However, the *in situ* doping method often requires high temperatures and complex processes, and the chemical reagents are poisonous.

It is rare to discuss the yield rates of N-doped carbon nanomaterials, which should be carefully investigated in the future when considering their practical applications. In contrast to the post-treatment strategy with a surplus supply of nitrogen, *in situ* doping is more effective because the synthesis of carbon nanomaterials and the N-doping takes place at the same time. Therefore, the *in situ* approach shows relatively higher yield rates, which represents an easy reactions which deserves more research.

For the *in situ* doping process, three main precursors of acetonitrile,[12] melamine[15] and polyacrylonitrile[16] were investigated the most, and the synthesis of carbon nanomaterials and N-doping had been simultaneously realized during the growth process. Acetonitrile was typically used in chemical vapor deposition (CVD) with copper foil as a catalyst to synthesize N-doped graphene (Fig. 1a). Melamine and polyacrylonitrile required higher temperatures in the synthesis of N-doped carbon nanomaterials. Gas molecules, such as carbon oxides (CO_x) and nitrogen oxides (NO_x), were side products of the pyrolysis, which led to the formation of mesoporous and microporous structures (Fig. 1b). For the post-treatment strategy, carbon frameworks were firstly synthesized before N-doping. Polymer and metal–organic frameworks represent the two most used carbon frameworks because of their easy synthesis and controllable porous structure. Subsequently, carbon frameworks were treated in the presence of various nitrogen sources such as ammonia (NH_3) or nitrogen gas (N_2) to realize the doping of nitrogen (Fig. 1c).[17]

3. N-Doped carbon nanomaterials for lithium ion batteries

Lithium ion batteries have been extensively explored for use as the main type of energy storage devices since their production by the Sony Corporation in the 1990s, and the rapid development of electrical vehicles and smart grids have urged further advances by increasing their energy density and rate capability. To this end, a variety of electrode materials have been widely investigated over the past decades. Carbon nanomaterials such as graphene,[18,19] CNTs,[2,20] CNFs[21] and activated carbon were mostly studied as electrode materials to fabricate LIBs based on their high electrical conductivities, mechanical strengths and specific areas. However, the low energy storage capability and poor electrochemical activity based on the instinctive lithium storage mechanism of bare carbon materials have hindered their further applications. To this end, N-doped carbon nanomaterials have been mostly explored as the main type of promising anode materials to enhance LIBs because nitrogen atoms are more electronegative than carbon atoms and give stronger interactions with Li ions as mentioned previously.[22] Furthermore, the defects introduced by N-doping provided more channels for Li ions and electrolytes for diffusion as well as more sites for lithium storage.[23,24]

The main challenge of using CNTs in LIBs lies in their low specific capacities. Although active materials such as metal oxides have been introduced to improve their electrochemical performances,[25,26] these guest materials tend to aggregate instead of being uniformly dispersed, which often resulted in low stability. Based on a plasma enhanced CVD method, N-doped CNTs had been synthesized to greatly enhance the energy storage capability, as the incorporation of nitrogen atoms effectively generated extrinsic defects in the walls of CNTs to provide more active sites for binding with Li ions (Fig. 2a and b).[11] Interestingly, the N-doped CNT electrodes exhibited an anomalous phenomenon that the capacity increased with the cycle number (Fig. 2c). For example, at the C/4 rate, the capacity was about 340 mA h g^{-1} and may reach 1920 mA h g^{-1} after 200 charge–discharge cycles. It was found that Li ions diffused into the interwall space of the CNTs through the N-doped defects in the walls, which provided more space for Li storage (Fig. 2d). Recently, a re-growth CVD method was developed to synthesize N-doped CNT films by using bare CNT sheets as templates to form a core–sheath structure with the pristine CNT as the core and the N-doped graphene layers as the sheath (Fig. 2e and f).[7] The nitrogen content could be controlled well with a maximal value of 6 wt%. The resulting hybrid film was flexible, strong, and highly conducting. When it

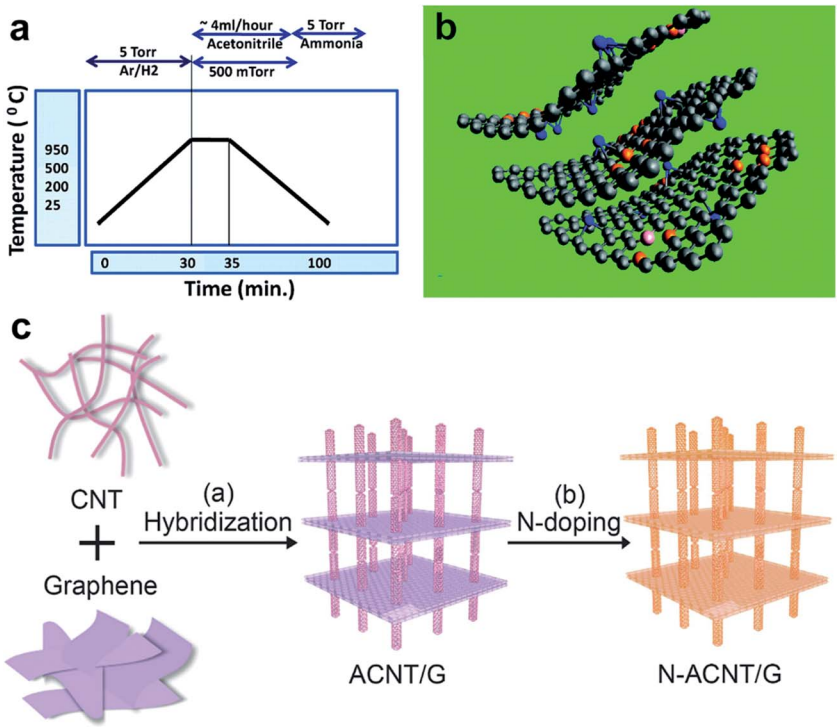

Fig. 1 (a) Schematic representation of the *in situ* doping process for the synthesis of N-doped carbon nanomaterials. (b) Schematic illustration of the N-doped graphene. (c) Schematic illustration of the synthesis of N-doped carbon nanomaterials by post-treatment. (a and b) Reproduced with permission.[12] Copyright 2010, American Chemical Society. (c) Reproduced with permission.[17] Copyright 2014, Wiley-VCH. ACNT/G: aligned carbon nanotube/graphene sandwich, N-ACNT/G: nitrogen-doped aligned carbon nanotube/graphene sandwich.

was used as an anode, a high specific capacity of 390 mA h g^{-1} was maintained after 200 cycles at 4C. In addition, the hybrid CNT films can be further assembled into flexible LIBs that worked effectively under bending and twisting (Fig. 2g). Note that the previously described N-doped CNTs were highly aligned with each other, so the charges can directly and effectively be

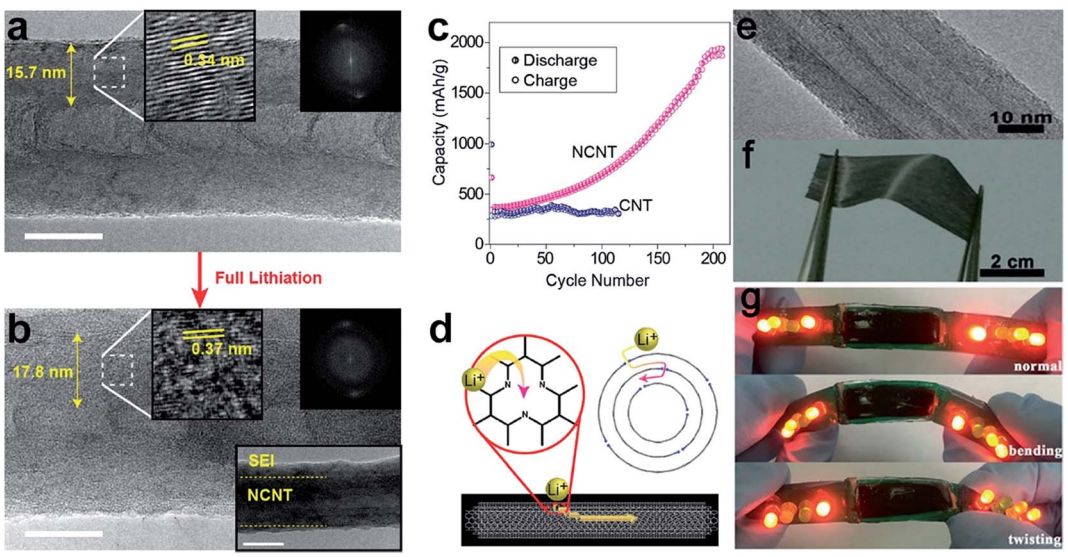

Fig. 2 (a and b) TEM images of an individual N-doped CNT at the same spot before and after lithiation, respectively. Scale bar, 20 nm. (c) Cycling performances of N-doped CNTs and commercial multi-walled CNTs. Current densities, 80 mA g^{-1}. (d) Schematic illustration of the insertion of lithium ions into the interwall space of N-doped CNTs through the wall defects. (e) TEM image of a multicore structure of N-doped CNT. (f) A free-standing N-doped CNT film. (g) Photographs of a flexible lithium ion battery to power light-emitting diodes (LEDs) before and after bending and twisting. The brightness of the LED remained stable during deformation. (a–d) Reproduced with permission.[11] Copyright 2012, American Chemical Society. (e and f) Reproduced with permission.[7] Copyright 2016, Wiley-VCH.

transported along their length (*i.e.*, the CNT-aligned direction) to contribute to the high energy storage capabilities. For the most studied disordered structures such as networks, the charge transport would encounter much longer pathways with low electronic and electrochemical properties.

Similarly, N-doped graphene can also be used as a promising electrode for LIBs. As partly discussed previously, there are three typical forms of nitrogen which exist in the N-doped carbon nanomaterials including graphene: pyridinic, pyrrolic/pyridine and quaternary (Fig. 3a).[24] Both pyridinic and quaternary nitrogen atoms are sp^2 hybridized to improve their electronic conductivity and they can introduce more defects and active sites in the carbon host, which can enhance the lithium storage capacity and rate capability of the electrode materials. For a typical synthesis where a copper foil was used as the catalyst and acetonitrile was used as the precursor,[12] the resulting N-doped graphene showed an enhanced capacity of ~70% compared with the bare graphene under the same conditions. Note that here the high content of pyridinic nitrogen atoms played a critical role as they displayed a higher binding energy with the Li ion and lower Li diffusion and desorption barrier.

The most important advantage of the N-doped graphene as an electrode material for LIBs lies in the superior charge and discharge performance. For example, for the graphene material synthesized using a post-treatment method by heating the original graphene powder under a mixed gas of NH_3 and argon (Ar), the doped graphene electrodes can be fully charged in tens of seconds at a high current density.[8] At a high current rate of 25 A g^{-1}, the N-doped graphene electrode also showed a high capacity of ~209 mA h g^{-1}. The high electrochemical performance of the N-doped graphene can be mainly explained by the fact that both its electrical conductivity and electrochemical activity are simultaneously enhanced during the doping process, which is favorable for the lithium ion diffusion and electron transport in the charge–discharge process. Additionally, the doping process has also greatly increased its disordered structure which gives better electrochemical properties.[27]

Differently from the previously described post-treatment method, the synthesis of graphene and nitrogen doping were simultaneously achieved using a hydrothermal method.[13] The hydrothermal method is more convenient and energy saving in comparison to using the CVD method, because the latter requires high temperatures and complicated processes. However, the nitrogen content of the resulting N-doped graphene is typically much lower. When it was used as the anode material to fabricate LIBs, a reversible capacity of 655 mA h g^{-1} was produced at 0.1 A g^{-1}, which can be maintained by increasing the current density from 0.1 A g^{-1} to 5 A g^{-1} and further recovered upon decreasing the current density to 0.1 A g^{-1}.

Supramolecular polymerization has been used to synthesize N-doped porous graphene materials by using graphene oxide@melamine cyanurate as the precursor.[28] Melamine

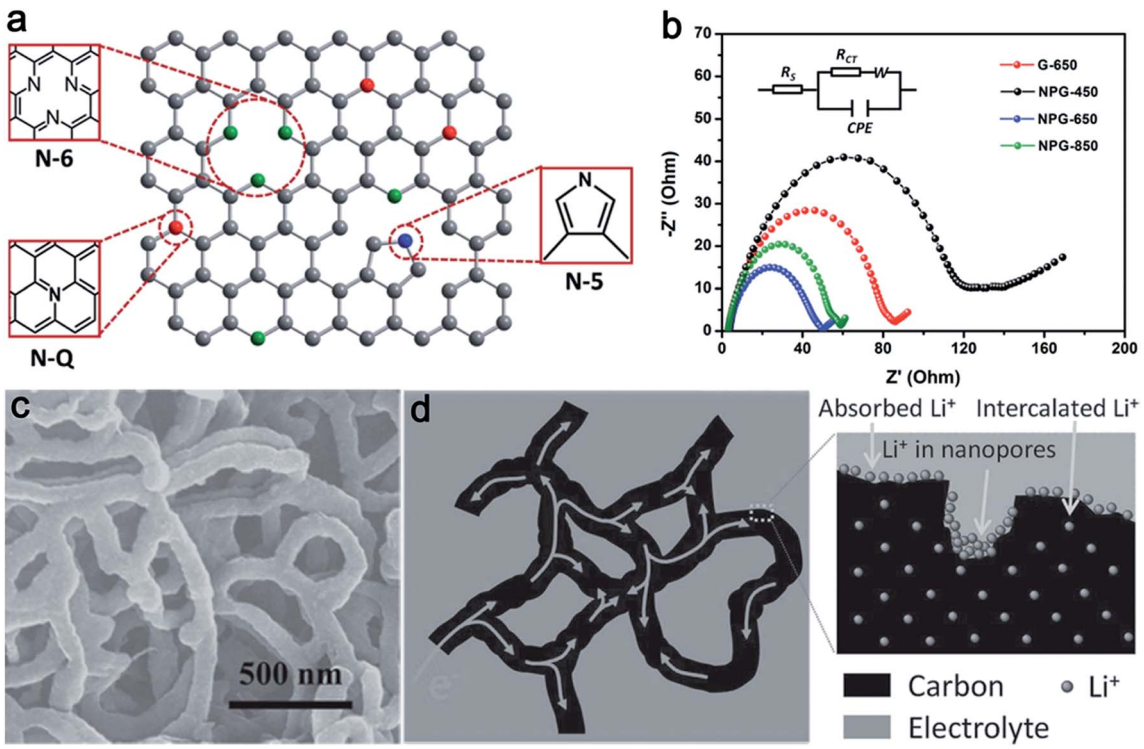

Fig. 3 (a) Schematic illustration of the forms of nitrogen in N-doped carbon nanomaterials. (b) Nyquist plots of the non-doped graphene (G-650) and N-doped graphene with different annealing temperatures of NPG-450 (450 °C), NPG-650 (650 °C), and NPG-850 (850 °C). (c) SEM image of the N-doped CNF network. (d) Schematic representation of electron transmission and Li ion storage in the N-doped CNF network. (a, c and d) Reproduced with permission.[24] Copyright 2014, Royal Society of Chemistry. (b) Reproduced with permission.[28] Copyright 2015, Wiley-VCH. NPG: nitrogen porous graphene sheet, SEM: scanning electron microscopy.

cyanurate functioned as a separator to prevent the re-stacking of the graphene sheets, a template to produce the porous structures and a source of doped nitrogen. The nitrogen contents were controlled using the annealing temperature and reached the highest value of 18.8 at% at 450 °C. According to the electrochemical impedance spectroscopy results, the nitrogen doping and porous structure offered higher electrolyte accessibility and better charge transport capability compared with the non-doped graphene (Fig. 3b). A specific capacity of 900 mA h g^{-1} was maintained after 150 cycles when the resulting N-doped graphene was used as the anode in a LIB. N-Doped graphene nanoribbons have been also synthesized after longitudinal unzipping of N-doped CNTs using nitric acid oxidation.[29] Because of the nitrogen doping and abundant edges, the N-doped graphene nanoribbons exhibited a high rate capability at high current densities of 0.3 A g^{-1} to 3 A g^{-1}.

Besides CNT and graphene, other carbon nanomaterials such as CNF,[9,24] porous carbon[30–32] and biomass derived carbon[33,34] can also be doped with nitrogen to make LIBs. N-Doped porous CNF networks have been synthesized by using polyacrylonitrile and melamine as precursors (Fig. 3c).[24] The highest nitrogen content reached 7.3 at%, and the content of chemically active pyridinic nitrogen was 38.38%. The N-doped CNF anode exhibited a reversible capacity of 1323 mA h g^{-1} at 50 mA g^{-1} with both high cycling stability and rate capability. The CNFs served as channels for electron transport, whereas a number of nanopores among the CNFs acted as reservoirs for the storage of lithium ions (Fig. 3d). N-Doped mesoporous carbon (N-MC) was synthesized by pyrolyzing gelatin between 700 °C and 900 °C from a nano-$CaCO_3$ template.[30] The as-synthesized N-MC had pore diameters from 25 nm to 30 nm, which favored the diffusion of electrolytes and ions. The content of pyridinic nitrogen and the capacity decreased with the increasing pyrolyzing temperature, whereas the highest capacity of 1029 mA h g^{-1} was observed at 700 °C. Sustainable biomaterials with high contents of proteins represent a type of promising alternative of the relatively expensive carbon precursors in synthesizing N-doped carbon nanomaterials. For example, egg white was used as the precursor to make protein-derived mesoporous carbon (P-MC).[33] The highest nitrogen content of 10.12 wt% was achieved at a low temperature of 650 °C, whereas the lowest nitrogen content of 6.04 wt% was obtained at a relatively high temperature of 850 °C. Note that the fourth type of nitrogen atom, oxidized nitrogen, was detected in this P-MC. A high reversible lithium storage capacity of 1780 mA h g^{-1} was discovered when the P-MC was used as the electrode material. However, the nitrogen content was reduced to 1.8% after further heating at 1100 °C, and a much lower reversible capacity of 716 mA h g^{-1} was produced, which indicated the significance of a high nitrogen content for the realization of high-performance LIBs. Also, a type of N-doped porous carbon nanomaterial was successfully synthesized from the shells of broad beans, and a discharge capacity of 261.5 mA h g^{-1} was achieved after 200 cycles when applied as an anode in LIBs.[35]

Except from being directly used as electrode materials, N-doped carbon nanomaterials can also be used as additives or electrode substrates in LIBs. Suffering from poor conductivity and structural stability, transition metals and transition metal sulfides exhibited fast capacity fading and poor cycling stability in LIBs. For example, molybdenum disulfide (MoS_2) has been suggested as a promising anode material for LIBs with a high specific capacity. A hybrid hollow structure was synthesized by growing ultrathin MoS_2 nanosheets on N-doped carbon nanoboxes.[36] The introduction of N-doped carbon nanomaterials can greatly improve the conductivity of the composite electrode and the hollow structure of carbon nanoboxes can effectively alleviate the strain caused by the volume change during cycling. Therefore, the designed hybrid electrode showed a high specific capacity of 824 mA h g^{-1} at 1.0 A g^{-1} and high cycling stability up to 200 cycles.

With a layered structure, the electrochemical performances of MoS_2 can be controlled by designing a specific electrode structure. The unique intercalated nanostructure efficiently combined the advantages of N-doped carbon nanomaterials and transition metal sulfides, such as high electrical conductivity and high electrochemical activity, respectively.[37] A N-doped microporous carbon nanofilm/MoS_2 composite has been synthesized with an alternating layer-by-layer nanostructure. The intercalated nanostructure can simultaneously enlarge the active reaction sites for lithium ions and prevent the aggregation of MoS_2 layers. So, this composite electrode showed a high capacity of 1190 mA h g^{-1} after 500 cycles at 1.0 A g^{-1}, which was considerably higher than those of the N-doped carbon nanofilm ($\sim$300 mA h g^{-1}) and MoS_2 electrodes ($\sim$10 mA h g^{-1}).[38] To summarize, N-doped carbon nanomaterials can provide high capacities when applied as anodes for LIBs. Low cost and high efficiency preparation methods should be developed so that commercial applications can be realized.

4. N-Doped carbon nanomaterials for lithium–sulfur batteries

Because of the relatively high theoretical specific capacity of sulfur (1675 mA h g^{-1}), the lithium–sulfur battery has attracted more and more attention over the past few decades.[39] However, there are several obstacles in the way before there are practical applications of lithium–sulfur batteries.[40] Firstly, the instinctive insulation of sulfur is unfavorable for electrode materials especially under operation at high current densities. Secondly, the dissolution of intermediate polysulfides in the electrolyte leads to the loss of active materials and the polysulfide shuttle phenomenon, which results in a fading capacity and low coulombic efficiency. Thirdly, the large volume expansion during discharging often leads to poor stability of the lithium–sulfur batteries. The synthesis of carbon/sulfur composite material was verified as a promising strategy to solve the previously described problems.[41] It is different from the direct use as an electrode in LIBs reviewed in this paper, carbon nanomaterials have been mainly used as additives in lithium–sulfur batteries. The incorporation of highly conductive additives such as N-doped graphene and CNTs can greatly enhance

the conductivity of the sulfur electrode. It is also worth noting that in lithium–sulfur batteries, the test voltage ranged from 1.7 V to 2.8 V, and the carbon materials contribute very little to the total capacity at this voltage window. The three dimensional (3D) carbon-based porous framework had been widely designed for the lithium–sulfur batteries as such a unique structure can provide pathways for electron transport,[42,43] whereas the micro/mesopores may accommodate the volume expansion during discharging.[44,45]

The heteroatoms can further lead to a stronger surface interaction with polysulfides and immobilize the sulfur and intermediates polysulfides, which can greatly improve the electrochemical performance of lithium–sulfur batteries (Fig. 4a).[46,47] Typically, a solvothermal process was used to synthesize the 3D N-doped graphene framework using NH_3 as the nitrogen source.[48] Typically, 10.1 at% carbon atoms were substituted by the nitrogen atoms. The as-synthesized 3D N-doped graphene showed a high specific surface area of 398 $m^2\ g^{-1}$ with pore sizes of about 4 nm.[45] Besides high electrical conductivity and effective transport channel, the N-doped carbon framework also provided strong adsorption abilities for polysulfides to accommodate high sulfur loading (Fig. 4b).[49] The sulfur content determines the capacity of the sulfur cathode materials, and a high sulfur loading is a promising way to improve the performance of lithium–sulfur batteries. By using a N,S-doped graphene framework as a 3D current collector, the active materials loading could reach as high as 4.6 mg cm^{-2}. The discharge capacity for the N,S-doped graphene electrode was about 675 mA h g^{-1} at 1C. With a further increase of the active materials loading from 4.6 mg cm^{-2} to 8.5 mg cm^{-2}, the reversible discharge capacity could reach approximately 700 mA h g^{-1} at 1C.[49] A high content of sulfur (87.6 wt%) can be obtained by using a 3D N-doped graphene framework, which was almost the highest content in the reported electrodes. The as-designed 3D composite electrode exhibited both high rate capability and cyclability with a reversible specific capacity of 1483 mA h g^{-1} at 100 mA g^{-1}.[48]

Nitrogen doping also promoted the chemical bonding between the nitrogen and oxygen functional groups on carbon, which was favorable for the uniform distribution and re-deposition of sulfur into the carbon host to improve the cycling performance.[50] For the N-doped graphene synthesized using thermal nitridation of a graphene oxide (GO) framework under a NH_3 atmosphere, the oxygenated functional groups on the GO sheets were decomposed and partially transformed to the N-containing groups, resulting in a N content of ~3.9 wt% or 3.7 at%.[10] This N-doped graphene framework demonstrated a hierarchically porous structure with pore sizes of 5 nm and 10–30 nm, which were beneficial as the smaller pores immobilized the intermediate whereas the larger pores facilitated the diffusion of electrolytes. Therefore, the resulting cathode exhibited a high rate capability and ultra-long cycle performance up to 2000 cycles with a decay rate of 0.028% per cycle at 2C.

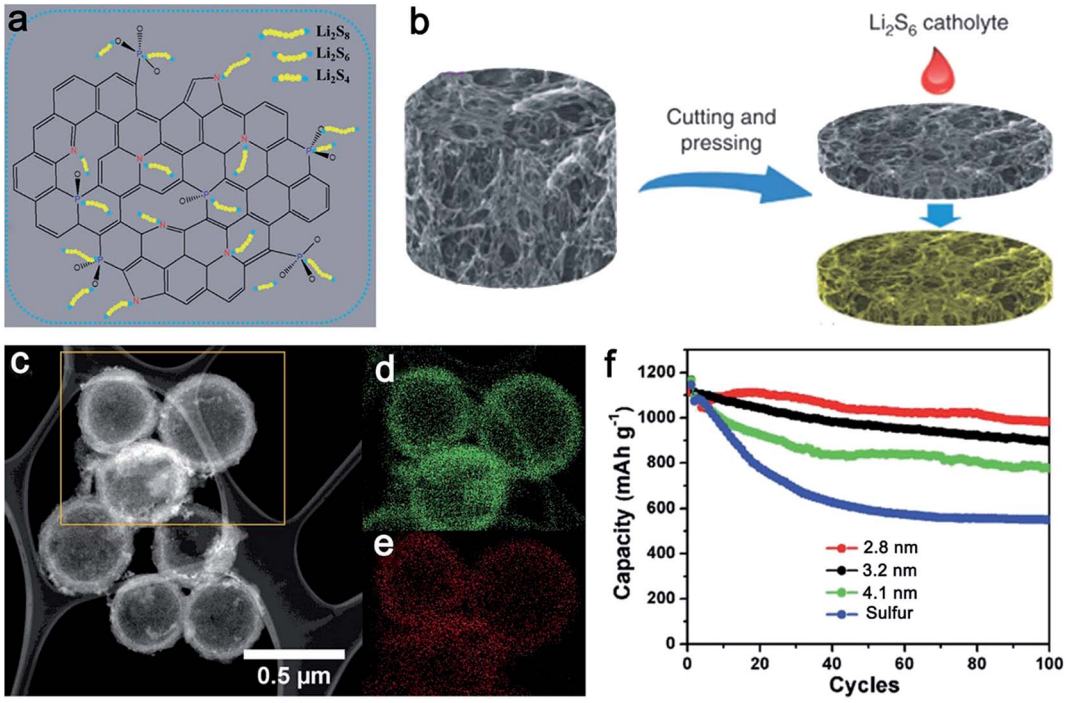

Fig. 4 (a) A schematic illustration of the polysulfide adsorption at the heteroatom (N and P) doped carbon nanomaterials. (b) A lightweight N-doped graphene framework used for the fabrication of lithium–sulfur battery electrodes after adding polysulfide. (c) An SEM image of the N-doped mesoporous hollow carbon nanospheres. (d and e) Elemental mapping of carbon and sulfur of the region shown in the square frame of (c). (f) Discharge capacity *versus* cycle number for the N-doped mesoporous carbon materials with different diameters. (a) Reproduced with permission.[47] Copyright 2015, Royal Society of Chemistry. (b) Reproduced with permission.[49] Copyright 2015, Nature Publishing Group. (c–f) Reproduced with permission.[11] Copyright 2015, Wiley-VCH.

More importantly, the self-aggregation and re-stacking of carbon nanomaterials can be mitigated with unexpected excellent properties.[51] For example, a well-defined N-doped CNT/graphene sandwiched structure was designed using a two-step CVD process, which provided efficient 3D electron transfer pathways and ion diffusion channels.[52] The N-doping process introduced more defects and active sites to the hybrid materials, which can greatly enhance the cyclic and rate performance of the cathode materials for the lithium–sulfur batteries. A high initial reversible capacity of 1152 mA h g^{-1} was available at 1C, whereas a reversible capacity of ~770 mA h g^{-1} had been achieved at 5C. Subsequently, a simple solid-state growth strategy was designed to synthesize highly N-doped CNT/graphene 3D nanostructure without using the CVD process.[53] Compared with the CVD method, this new strategy used a nickel foam as the catalyst with CNTs being grown on both sides of the nickel foam to form a 3D nanostructure. Because of the interconnected 3D nanostructure (mesopores of 2–5 nm and 10 nm) and high nitrogen doping (12.5 wt%), a high coulombic efficiency was achieved, after the first cycle it was 101% at 0.1C. Furthermore, good stability was also achieved at a high rate of 2C, showing a high capacity of 896 mA h g^{-1} after 200 cycles.

Apart from the N-doped CNT and graphene, N-MC or CNF with hollow or porous structures have also been prepared for use in lithium–sulfur batteries.[50] For example, N-doped porous CNF/S composites were prepared as the cathode materials for lithium–sulfur batteries.[54] Because of the unique one dimensional (1D) porous nanostructure, these composites allowed fast electron transport and possessed high surface areas to effectively immobilize the sulfur. Furthermore, nitrogen doping can further enhance the adsorption of polysulfide on the surface of N-doped CNF networks, which exhibited high capacity reversibility and long cycle stability. When they were used as the cathode in the lithium–sulfur batteries, a high specific discharge capacity of 749 mA h g^{-1} at 0.2C was produced after 180 cycles. However, it was unclear about the favorable pore size confining the sulfur. To this end, N-doped carbon nanospheres with different pore sizes of 4.1, 3.2 and 2.8 nm were compared.[55] The introduction of nitrogen better immobilized the polysulfides through the coordination interaction with nitrogen (Fig. 4c–e). The pore size of 2.8 nm displayed the highest capability and best cycling performance (Fig. 4f), which can be attributed to the better encapsulation and confinement of the porous carbon shell for sulfur/polysulfides. It is proposed that melted sulfur would diffuse into the shell, which was inversely proportional to the pore size, by capillarity. To summarize, the content of sulfur greatly influences the overall volumetric capacity and energy density of the cathode. For lithium–sulfur batteries, N-doped carbon nanomaterials can provide a stronger intercalation with lithium polysulfide, compared to that with bare carbon nanomaterials, to suppress the shuttle effect. The better dispersion of N-doped carbon nanomaterials can synchronously improve the loading of sulfur and show an excellent electrochemical performance. Furthermore, the composite of N-doped carbon nanomaterials with transition metal oxides and sulfides represents a promising candidate for the electrode materials.

5. N-Doped carbon nanomaterials for metal–air batteries

N-Doped carbon nanomaterials can also be used as electrode materials in metal–air batteries because of their high surface area, porosity and electrocatalytic activity. Metal–air batteries, including the Li–air battery,[56,57] the zinc (Zn)–air battery[58] and the aluminium–air battery,[59] have recently attracted increasing interest because of their superior capacities. In a conventional metal–air battery, the metal anode is electrochemically coupled to oxygen by an air cathode. During the discharge process, metal ions flow from the anode through an electrolyte and react with oxygen at the cathode with use of special catalysts (Fig. 5a). The electrochemical performance of metal–air batteries has mainly been limited by the air cathode that was the catalyst for the oxygen reduction reaction.[60,61] The high cost and poor long-term stability have hindered the commercial application of the platinum/carbon (Pt/C) catalyst. Developing metal-free and carbon-based catalysts thus represents a promising strategy as a substitution for the Pt-based catalyst.[62] A theoretical calculation had revealed that N-doping was an effective method to achieve high-performance oxygen reduction reaction catalysts for use as a cathode materials. It is commonly accepted that a pyridinic or graphitic nitrogen atom can induce a positive charge on the adjacent carbon atoms, which favors the absorption of oxygen and fracture of the O–O bond. The high activity can be attributed to the larger electronegativity of N (3.04) compared to the C atom (2.55) and the formation of positive charge density on the adjacent C atom.[63] Under this guidance, N-doped carbon nanomaterials with high activities and porous structures had been mostly studied for use as cathode materials for metal–air batteries.[64] The designed porous structure and high surface area facilitated the diffusion of electrolyte solution and transport of oxygen, which was of great importance in metal–air batteries. Furthermore, the high surface area was beneficial for high metal oxide uptake and provided more active sites for the electrocatalyst.[65] The recent progress with the N-doped carbon nanomaterials for metal–air batteries is summarized next.

The performance of the metal–air batteries mainly depends on the type, structure and morphology of the air electrode. In general, carbon nanomaterials are used as the cathodic catalyst in an air electrode and the electrochemical reactions occur on the carbon. Graphene shows both high electrochemical activity and stability towards an oxygen reduction reaction in alkaline solution. However, the catalytic activity in acid solution was relatively low, which may be ascribed to the low active sites of graphene in acid solution.[57] Nitrogen doping is an effective strategy for providing more active sites and improving electrochemical performance. Fig. 6a represents an early study in the development of the N-doped graphene catalyst for metal–air batteries.[66] The N-doped graphene sheets were synthesized by annealing pristine graphene sheets in an NH_3 atmosphere at high temperatures. The oxygen reduction reaction activity of the as-synthesized N-doped graphene sheet was tested using a rotating disk electrode. At a higher annealing temperature,

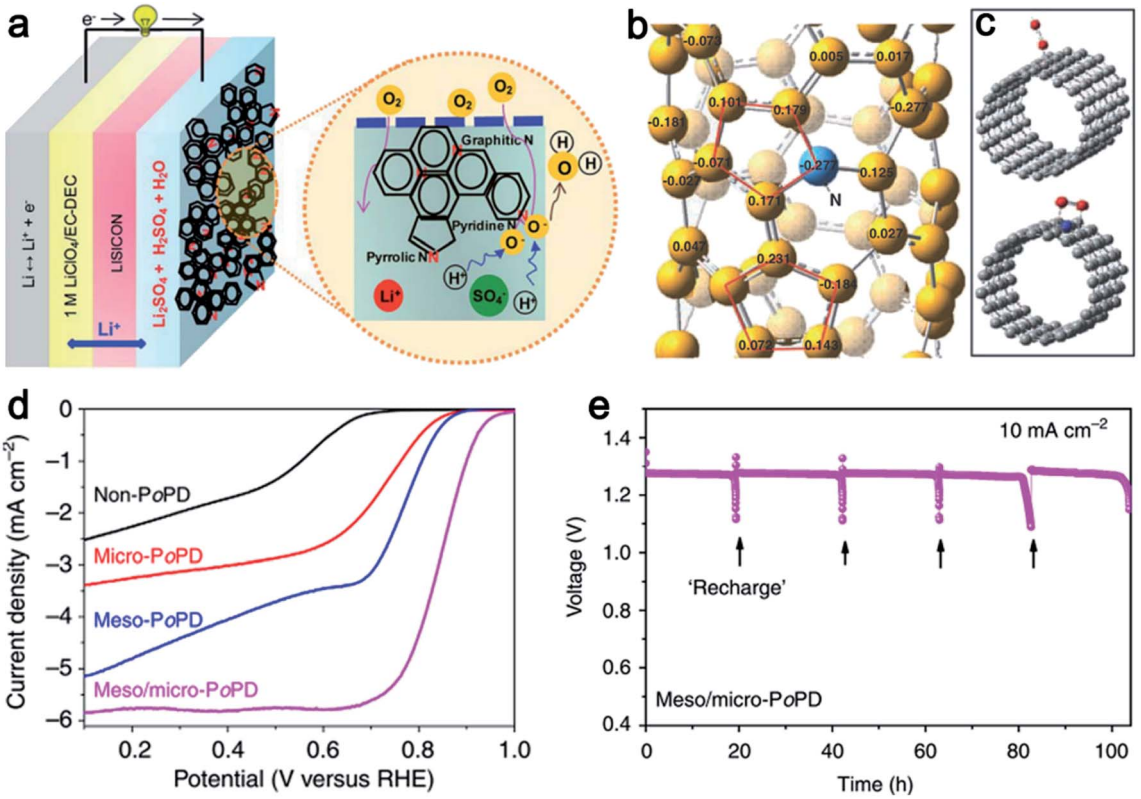

Fig. 5 (a) Schematic illustration of the use of N-doped graphene cathode for lithium–air battery. (b) Calculated charge density distribution of a N-doped CNT. (c) Schematic representations of possible adsorption modes of an oxygen molecule on the bare CNTs (top) and N-doped CNTs (bottom). (d) Oxygen reduction reaction polarization plots of meso/micro N-doped carbon and reference catalysts. The loading was 0.1 mg cm^{-2} for all materials. (e) "Recharging" the Zn–air battery by replenishing the Zn anode and electrolyte. The arrows indicate the "recharging" process. (a) Reproduced with permission.[62] Copyright 2012, Royal Society of Chemistry. (b and c) Reproduced with permission.[63] Copyright 2009, American Association for the Advancement of Science. (d and e) Reproduced with permission.[70] Copyright 2014, Nature Publishing Group.

a higher ratio of pyridine-type nitrogen formed which facilitated the oxygen reduction reaction, resulting in a higher discharge voltage and lower onset potential. For example, N-doped graphene sheets annealed at 850 °C showed the highest discharge voltage of 3.6 V *versus* Li^+/Li, which was only 0.15 V lower than that of the commercial 20 wt% Pt/carbon black catalyst. Porous graphene frameworks with high surface areas and large porosities had been further synthesized for both enhanced electrode–electrolyte interactions and electrolyte–reactant diffusions, which were critical for high-performance cathodes in metal–air batteries.[64] They exhibited a high stability in alkaline solution with a small shift of only about 15 mV after 5000 cycles, which was comparable to the shift obtained with the commercial 20 wt% Pt/carbon black catalyst. Even in an acidic solution, this catalyst showed no activity loss for the oxygen reduction reaction in the presence of methanol, indicating a high tolerance to methanol poisoning effects.

Nitrogen-doping had been demonstrated to improve the catalytic performances of CNTs. For example, vertically aligned N-doped CNTs acted as a metal-free electrode with a much better electrocatalytic activity than Pt for the oxygen reduction reaction in alkaline solutions. Theoretical calculations indicated that the C atoms adjacent to N-dopants possessed a substantially high positive charge density to counterbalance the strong electronic affinity of the N atom (Fig. 5b).[67] Furthermore, the nitrogen-induced charge delocalization could also change the chemisorption mode of O_2 from the usual end-on adsorption to a side-on adsorption (Fig. 5c). The parallel diatomic adsorption could effectively weaken the O–O bonding to enhance the oxygen reduction reaction of the N-doped CNT electrodes, which exhibited higher activity in catalysing the electrochemical reduction of O_2. N-Doped CNTs with different amounts of nitrogen can be used as cathodes in lithium–O_2 batteries.[68] The discharge capacities were increased with the increasing nitrogen content in N-doped CNTs, and the highest value occurred at 7906 mA h g^{-1} at 0.1 mA cm^{-2}. Another important parameter for evaluating metal–air batteries is the over potential, the difference between the discharge plateau and charge plateau. The lower the over potential is, the better the catalysis achieved. For the as-synthesized N-doped CNT, the over potential was lower than that of bare CNTs, and the over potential decreased when the nitrogen contents were increased. It was found that the discharge products were more uniformly distributed in N-doped CNTs, which could be more easily decomposed to enhance the cyclic performance. Similarly, the N-doped CNTs also exhibited excellent catalytic activities as air cathodes for Zn–air batteries.[69]

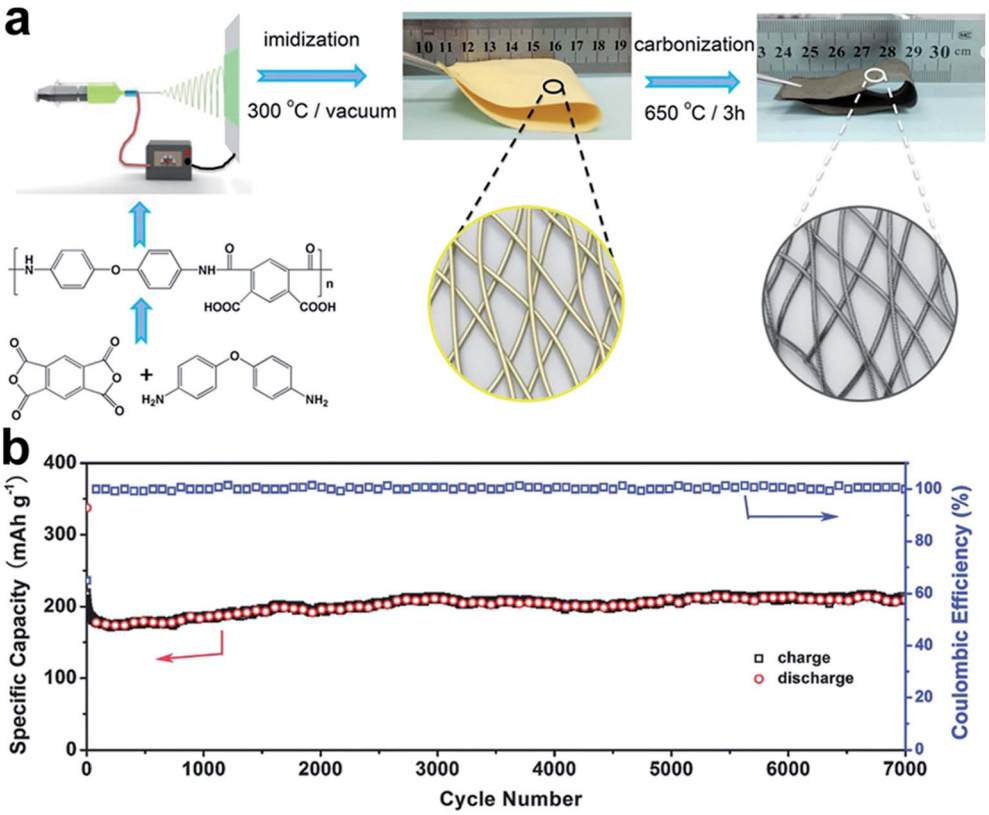

Fig. 6 (a) Schematic illustration of the fabrication of highly flexible N-doped CNF films. (b) Ultra-long cycling performance of the N-doped CNF at a current density of 5 A g^{-1}. (a and b) Reproduced with permission.[89] Copyright 2016, Wiley-VCH.

Besides the N-doped graphene and CNT, a variety of N-doped carbon nanomaterials such as N-doped CNF,[70,71] carbon nanoparticles,[72] onion like carbon[73] and porous carbon[74] had also been synthesized using various methods for the improvement in the oxygen reduction reaction activity. For example, a coral-like N-doped CNF array was obtained using stainless steel as the substrate. The vertically aligned, coral-like N-doped microstructure had a nitrogen content of 3.1 at%.[71] When it was used as the air electrode for lithium–air batteries, a very low over potential of 0.3 V at a current density of 100 mA g^{-1} was achieved, and a high specific capacity of 1000 mA h g^{-1} could also be produced. The full capacity of this material was measured by discharging the cell down to 2.2 V at 500 mA g^{-1}, and an ultra-high capacity of over 40 000 mA h g^{-1} was achieved after discharging for 100 h. It should be noted that the discharge product of the N-doped carbon fiber was lithium peroxide (Li_2O_2), which had been confirmed using selected area electron diffraction. The unique onion like N-doped carbon showed a high specific surface area of 406.4 m^2 g^{-1} and a porous structure with a pore diameter of 20 nm. When it was used in lithium–air batteries, the over potential was 0.88 V with discharge and charge potentials of 0.71 and 0.17 V, respectively, resulting in a round-up efficiency of 76%. When tested at a fixed cut-off capacity, this onion like carbon had an efficiency of 70.0% after 194 cycles, indicating a good cyclic stability.[73]

Hierarchically N-doped porous carbon materials were prepared using a hard templating method to simultaneously optimize both porous structures and surface properties.[74] The unique structure with a meso/micro multimodal pore size distribution led to the highest oxygen reduction reaction activity in alkaline media. The as-prepared catalysts exhibited a high specific surface area of 1280 m^2 g^{-1}, which can supply numerous accessible active sites for oxygen reduction. The rotating disk electrode measurements showed that porous N-doped carbon catalysts had a comparable oxygen reduction reaction activity to the Pt/carbon black catalyst with the same loading of 0.1 mg cm^{-2} (Fig. 5d). It can be used as an air electrode to construct a Zn–air battery, which outperformed the commercial Pt/carbon black catalyst. By refueling the Zn anode and electrolyte periodically, the air electrode could work robustly for more than 100 h without loss of voltage (Fig. 5e).

Except as the cathodic catalyst materials, N-doped carbon nanomaterials with high conductivity and porosity can also be used as additive materials to load noble metals, transition metal nitrides or metal oxide catalysts for metal–air batteries.[75–78] Bulk catalysts, such as molybdenum nitride and manganese dioxide, usually exhibit a limited oxygen reduction reaction activity because of their large particle sizes and low specific surface areas. Molybdenum nitride/N-doped carbon nanospheres were designed to improve the catalytic activity. These composite nanospheres enlarged the surface active sites and enhanced the electrocatalytic activity, which indicated it was a promising cathode catalyst for lithium–air batteries.[75] Also, N-doped carbon nanomaterials can greatly enhance the stability of

metal oxide catalysts. For example, ruthenium oxide (RuO_2) had been found to be one of the most effective catalysts to reduce the charge potentials of lithium–air batteries. However, the poor stability of RuO_2 nanoparticles resulted in limited charge/discharge cycles with low charge overpotentials. A 3D nanoporous cathode was developed by using N-doped graphene to stabilize the RuO_2 nanoparticles.[76] The RuO_2 nanoparticles were homogeneously dispersed between the inner and outer layers of the N-doped graphene with sizes of 3–5 nm, which can be directly used as a cathode in the lithium–air batteries. A large discharge capacity of 8700 mA h g^{-1} can be fully recharged at the highest recharge potential of 4.05 V. More importantly, the cathode had much better cycling stability with retained low charge potentials, and the cycling lifetime can reach more than 110 cycles with stable low charge potentials below 4.05 V. To summarize, N-doped carbon nanomaterials were studied for use as cathodic catalysts and additive materials in metal–air batteries. The mechanism of the catalyst effect of N-doped carbon nanomaterials remains unclear. The use of *in situ* transmission electron microscopy (TEM) and computational simulation might be helpful in understanding this mechanism.

6. N-Doped carbon nanomaterials for sodium-ion batteries

In spite of the broad applications of LIBs in human lives, the scarcity and high cost of lithium metal has been ringing alarm bells. Recently, SIBs have been widely studied and regarded as an alternative for LIBs because of the abundance and low cost of sodium metal.[79–82] Because of the relatively larger diameter of the Na ion, the electrochemical performances of SIBs are strongly dependent on the morphology and pore size of the electrode materials.[82] The use of a commercialized graphite anode in LIBs proved a failure because Na ions cannot effectively intercalate into the interlayer spacing between two graphene layers. More importantly, carbon nanomaterials such as CNT,[83] graphene,[84] carbon spheres[85] and porous carbon[86] have been found to facilitate the insertion/extraction of Na ions as the anode materials of SIBs. Previous studies proved that N-doping could generate extrinsic defects and enhance the electrical conductivities of carbon nanomaterials, which were favorable for improving the electrochemical performances of SIBs.

Use of graphene has been widely studied in LIBs, so it may also be suitable for use in SIBs. The morphology and pore size of graphene materials play important roles in regulating the ion transport and storage in SIBs.[87] For example, N-doped graphene foams with a well-defined 3D pore structure were used for SIBSs.[88] The combination of 3D structure and N-doping significantly improved the overall performance of SIBs. The N-doping can enlarge the lattice spacing and defects between two neighboring graphene layers, which effectively facilitated the diffusion of Na ions. Using the 3D N-doped graphene as the anode material, the resultant SIB showed a high initial reversible capacity of 852.6 mA h g^{-1} at 1C, which can be further maintained at ~70% after 150 cycles. However, the rate capability and long-term cycling performance of the anode materials need to be further improved to satisfy the practical applications. Electrospinning was used to synthesize N-doped CNF films, using polyamic acid as the polymer precursor. The N-doped CNF films were obtained by carbonating the polymer-based nanofibers, which resulted in a large number of pores being obtained during the thermal treatment (Fig. 6a).[89] The resulting N-doped CNF film showed a 3D fibrous network structure with multiscale nanopores, high N-doping level, high structural durability, and high mechanical flexibility. This unique nanostructure was favorable for the contact of electrolyte and ions, which can effectively facilitate the insertion/extraction of sodium ions. These materials exhibited a high rate capability with a capacity of 210 mA h g^{-1} after cycling for 7000 times at a current density of 5 A g^{-1}, which corresponded to a capacity retention of 99% (Fig. 6b). The superior rate capability and ultra-long cycling stability were attributed to the 3D interconnected conductive structure and the uniform distribution of micropores with a high nitrogen content. Recently, researchers have a biomass by-product, okra, as a natural nitrogen precursor to synthesize high content N-doped carbon materials.[90] When they were used as the anode of SIBs, a high coulombic efficiency of nearly 100% and much higher energy density than that obtained with the conventional hard carbon and CNFs had been simultaneously achieved. This research provided a sustainable and low-cost strategy to make high performance electrode materials for SIBs.

Similar to the LIBs, N-doped carbon nanomaterials can also work as additives or substrates of the electrode for SIBs. Metals and alloys are considered to be promising candidates for SIBs because of the high theoretical capacity, but they also have a large volume expansion in the charge–discharge process.[91] The design of metal/carbon composition provides an effective strategy for fabricating high performance electrodes. For example, amorphous red phosphorus confined in a metal–organic-framework-derived N-doped microporous carbon substrate was studied as an anode for SIBs.[92] A high reversible capacity up to 600 mA h g^{-1} was achieved at 150 mA g^{-1}, with an improved stability (450 mA h g^{-1} at 1 A g^{-1} after 1000 cycles), which benefited from the highly conductive pathways of electrons and good surface wettability provided by the high N-doping (15.5 wt%). Furthermore, simultaneously controlling the particle size of metal materials and ensuring that sufficient metal content had been used, improved the electrochemical performances of metal/carbon composite electrodes. Ultra small tin (Sn) nanodots can be encapsulated in N-doped carbon nanofibers using electrospinning and thermal treatment, which delivered a reversible capacity as high as 633 mA h g^{-1} at the current density of 200 mA g^{-1}. In this composite, the porous N-doped carbon frame not only facilitated the electron and Na ion diffusions, but also buffered the large volume fluctuation of Sn nanodots and prevented their pulverization and aggregation.[93] To summarize, differently from the LIBs, N-doped carbon nanomaterials did not show high capacity and stability when used in SIBs. Because of the larger diameter of the Na ions, it requires more effort to develop the suitable N-doped carbon nanomaterials for their application in SIBs.

7. Conclusion and expectations

Based on the morphologies of N-doped carbon nanomaterials, they can be divided into 1D N-doped CNTs, two-dimensional N-doped graphene and 3D N-doped frameworks. Each has its advantages and disadvantages. N-doped CNTs demonstrate high electrical conductivity and mechanical strength inherited from the bare CNTs. N-Doped graphene shows a large surface area with high catalytic sites at the edge. However, the synthesis of the two nanomaterials is relatively less efficient from a viewpoint of practical applications, and the restacking of N-doped graphene is also a key challenge. 3D N-doped frameworks are usually synthesized through the calcination of N-containing polymers, metal–organic-frameworks or biomass, which is more effective and with a lower cost. It is difficult to accurately control the microstructures and components of the N-doped frameworks.

Although N-doped carbon nanomaterials have been extensively studied as electrode materials for various batteries, there remain some challenges that need to be addressed in future studies. Firstly, a variety of synthetic methods have been widely investigated to synthesize N-doped carbon nanomaterials. However, it is still necessary to develop more effective methods to replace the conventional ones of CVD and post-treatment strategies at high temperature. Secondly, it is critical, although difficult to understand, the role of different types of nitrogen atoms. It has been reported that pyridinic nitrogen atoms favored lithium ion storage in LIBs,[94] pyridinic and pyrrolic nitrogen atoms showed stronger interactions with lithium polysulfide than quaternary nitrogen atoms,[95] and pyridinic and quaternary nitrogen atoms provided active sites for the oxygen reduction reaction in metal–air batteries.[66] However, it remains unclear about the working mechanisms behind these interactions. Thirdly, it is difficult to effectively tune both the content of nitrogen atoms and their ratios of different types of nitrogen. Generally, the use of lower temperature and higher nitrogen containing compounds results in higher nitrogen contents, but it remains challenging to accurately control the nitrogen content, and it is even more challenging to control the ratios of different nitrogen types.

Despite the remaining challenges and the necessity for further studies, N-doped carbon nanomaterials demonstrate great advantages for high power densities and long cycle performances, and they thus are promising materials for the advance of electrochemical batteries. It may be expected that they will dominate the electrode materials of batteries if their production and costs are competitive compared to their conventional counterparts.

Conflicts of interest

There are no conflicts to declare.

Acknowledgements

This work was supported by The Ministry of Science and Technology (MOST) (2016YFA0203302), the National Natural Science Foundation of China (NSFC) (21604012, 21634003, 51573027, 51673043, 21503079), Science and Technology Commission of Shanghai Municipality (STCSM) (18QA1400700, 16JC1400702, 17QA1400400, 15XD1500400, 15JC1490200) and Shanghai Municipal Education Commission (SHMEC) (2017-01-07-00-07-E00062).

References

1 P. G. Bruce, S. A. Freunberger, L. J. Hardwick and J. M. Tarascon, *Nat. Mater.*, 2011, **11**, 19–29.
2 S. W. Lee, N. Yabuuchi, B. M. Gallant, S. Chen, B. S. Kim, P. T. Hammond and Y. Shao-Horn, *Nat. Nanotechnol.*, 2010, **5**, 531–537.
3 H. Wang, Y. Yang, Y. Liang, L. F. Cui, H. Sanchez Casalongue, Y. Li, G. Hong, Y. Cui and H. Dai, *Angew. Chem., Int. Ed.*, 2011, **50**, 7364–7368.
4 N. Liu, Z. Lu, J. Zhao, M. T. McDowell, H. W. Lee, W. Zhao and Y. Cui, *Nat. Nanotechnol.*, 2014, **9**, 187–192.
5 G. Zheng, S. W. Lee, Z. Liang, H. W. Lee, K. Yan, H. Yao, H. Wang, W. Li, S. Chu and Y. Cui, *Nat. Nanotechnol.*, 2014, **9**, 618–623.
6 P. Chen, Y. Xu, S. He, X. Sun, S. Pan, J. Deng, D. Chen and H. Peng, *Nat. Nanotechnol.*, 2015, **10**, 1077–1083.
7 Z. Pan, J. Ren, G. Guan, X. Fang, B. Wang, S. G. Doo, I. H. Son, X. Huang and H. Peng, *Adv. Energy Mater.*, 2016, **6**, 1600271.
8 Z. S. Wu, W. Ren, L. Xu, F. Li and H. M. Cheng, *ACS Nano*, 2011, **5**, 5463–5471.
9 L. Qie, W. M. Chen, Z. H. Wang, Q. G. Shao, X. Li, L. X. Yuan, X. L. Hu, W. X. Zhang and Y. H. Huang, *Adv. Mater.*, 2012, **24**, 2047–2050.
10 Y. Qiu, W. Li, W. Zhao, G. Li, Y. Hou, M. Liu, L. Zhou, F. Ye, H. Li, Z. Wei, S. Yang, W. Duan, Y. Ye, J. Guo and Y. Zhang, *Nano Lett.*, 2014, **14**, 4821–4827.
11 W. H. Shin, H. M. Jeong, B. G. Kim, J. K. Kang and J. W. Choi, *Nano Lett.*, 2012, **12**, 2283–2288.
12 A. L. M. Reddy, A. Srivastava, S. R. Gowda, H. Gullapalli, M. Dubey and P. M. Ajayan, *ACS Nano*, 2010, **4**, 6337–6342.
13 Z. Xing, Z. Ju, Y. Zhao, J. Wan, Y. Zhu, Y. Qiang and Y. Qian, *Sci. Rep.*, 2016, **6**, 26146.
14 J. L. Liu, C. K. Poh, D. Zhan, L. Lai, S. H. Lim, L. Wang, X. Liu, N. G. Sahoo, C. Li, Z. X. Shen and J. Y. Lin, *Nano Energy*, 2013, **2**, 377–386.
15 X. C. Liu, S. M. Li, J. Mei, W. M. Lau, R. Mi, Y. C. Li, H. Liu and L. M. Liu, *J. Mater. Chem. A*, 2014, **2**, 14429–14438.
16 A. D. Roberts, S. X. Wang, X. Li and H. F. Zhang, *J. Mater. Chem. A*, 2014, **2**, 17787–17796.
17 C. Tang, Q. Zhang, M. Q. Zhao, J. Q. Huang, X. B. Cheng, G. L. Tian, H. J. Peng and F. Wei, *Adv. Mater.*, 2014, **26**, 6100–6105.
18 B. Z. Jang, C. Liu, D. Neff, Z. Yu, M. C. Wang, W. Xiong and A. Zhamu, *Nano Lett.*, 2011, **11**, 3785–3791.
19 N. Li, Z. Chen, W. Ren, F. Li and H. M. Cheng, *Proc. Natl. Acad. Sci. U. S. A.*, 2012, **109**, 17360–17365.
20 S. W. Lee, B. M. Gallant, Y. Lee, N. Yoshida, D. Y. Kim, Y. Yamada, S. Noda, A. Yamada and Y. Shao-Horn, *Energy Environ. Sci.*, 2012, **5**, 5437–5444.

21 L. F. Cui, L. Hu, J. W. Choi and Y. Cui, *ACS Nano*, 2010, **4**, 3671–3678.
22 H. M. Jeong, J. W. Lee, W. H. Shin, Y. J. Choi, H. J. Shin, J. K. Kang and J. W. Choi, *Nano Lett.*, 2011, **11**, 2472–2477.
23 X. Jia, G. Zhang, T. Wang, X. Zhu, F. Yang, Y. Li, Y. Lu and F. Wei, *J. Mater. Chem. A*, 2015, **3**, 15738–15744.
24 D. Nan, Z. H. Huang, R. Lv, L. Yang, J. G. Wang, W. Shen, Y. Lin, X. Yu, L. Ye, H. Sun and F. Kang, *J. Mater. Chem. A*, 2014, **2**, 19678–19684.
25 Y. Zhang, W. Bai, X. Cheng, J. Ren, W. Weng, P. Chen, X. Fang, Z. Zhang and H. Peng, *Angew. Chem., Int. Ed.*, 2014, **53**, 14564–14568.
26 J. Ren, Y. Zhang, W. Bai, X. Chen, Z. Zhang, X. Fang, W. Weng, Y. Wang and H. Peng, *Angew. Chem., Int. Ed.*, 2014, **53**, 7864–7869.
27 Z. Y. Sui, C. Wang, Q. S. Yang, K. Shu, Y. W. Liu, B. H. Han and G. G. Wallace, *J. Mater. Chem. A*, 2015, **3**, 18229–18237.
28 W. Ai, J. Jiang, J. Zhu, Z. Fan, Y. Wang, H. Zhang, W. Huang and T. Yu, *Adv. Energy Mater.*, 2015, **5**, 1500559.
29 Y. Liu, X. Wang, Y. Dong, Z. Wang, Z. Zhao and J. Qiu, *J. Mater. Chem. A*, 2014, **2**, 16832–16835.
30 Y. Mao, H. Duan, B. Xu, L. Zhang, Y. Hu, C. Zhao, Z. Wang, L. Chen and Y. Yang, *Energy Environ. Sci.*, 2012, **5**, 7950–7955.
31 A. D. Roberts, S. Wang, X. Li and H. Zhang, *J. Mater. Chem. A*, 2014, **2**, 17787–17796.
32 X. Wang, C. G. Liu, D. Neff, P. F. Fulvio, R. T. Mayes, A. Zhamu, Q. Fang, G. Chen, H. M. Meyer, B. Z. Jang and S. Dai, *J. Mater. Chem. A*, 2013, **1**, 7920–7926.
33 Z. Li, Z. Xu, X. Tan, H. Wang, C. M. B. Holt, T. Stephenson, B. C. Olsen and D. Mitlin, *Energy Environ. Sci.*, 2013, **6**, 871–878.
34 J. Ou, Y. Zhang, L. Chen, Q. Zhao, Y. Meng, Y. Guo and D. Xiao, *J. Mater. Chem. A*, 2015, **3**, 6534–6541.
35 G. Xu, J. Han, B. Ding, P. Nie, J. Pan, H. Dou, H. Li and X. Zhang, *Green Chem.*, 2015, **17**, 1668–1674.
36 X. Y. Yu, H. Hu, Y. Wang, H. Chen and X. W. Lou, *Angew. Chem., Int. Ed.*, 2015, **54**, 1–5.
37 B. Wang, Q. Wu, H. Sun, J. Zhang, J. Ren, Y. Luo, M. Wang and H. Peng, *J. Mater. Chem. A*, 2017, **5**, 925–930.
38 Z. Chen, H. Xie, L. Hu, M. Chen and L. Wu, *J. Mater. Chem. A*, 2017, **5**, 22726–22734.
39 H. Yao, G. Zheng, P. C. Hsu, D. Kong, J. J. Cha, W. Li, Z. W. Seh, M. T. McDowell, K. Yan, Z. Liang, V. K. Narasimhan and Y. Cui, *Nat. Commun.*, 2014, **5**, 3943.
40 Z. W. Seh, H. Wang, N. Liu, G. Zheng, W. Li, H. Yao and Y. Cui, *Chem. Sci.*, 2014, **5**, 1396–1400.
41 X. Ji, K. T. Lee and L. F. Nazar, *Nat. Mater.*, 2009, **8**, 500–506.
42 H. J. Peng, D. W. Wang, J. Q. Huang, X. B. Cheng, Z. Yuan, F. Wei and Q. Zhang, *Adv. Sci.*, 2016, **3**, 1500268.
43 J. L. Liu, L. Zhang, H. B. Wu, J. Lin, Z. X. Shen and X. W. Lou, *Energy Environ. Sci.*, 2014, **7**, 3709–3719.
44 H. J. Peng, J. Q. Huang, M. Q. Zhao, Q. Zhang, X. B. Cheng, X. Y. Liu, W. Z. Qian and F. Wei, *Adv. Funct. Mater.*, 2014, **24**, 2772–2781.
45 G. Zhou, L. C. Yin, D. W. Wang, L. Li, S. Pei, I. R. Gentle, F. Li and H. M. Cheng, *ACS Nano*, 2013, **7**, 5367–5375.
46 J. Song, M. L. Gordin, T. Xu, S. Chen, Z. Yu, H. Sohn, J. Lu, Y. Ren, Y. Duan and D. Wang, *Angew. Chem., Int. Ed.*, 2015, **54**, 4325–4329.
47 X. Gu, C. J. Tong, C. Lai, J. Qiu, X. Huang, W. Yang, B. Wen, L. M. Liu, Y. Hou and S. Zhang, *J. Mater. Chem. A*, 2015, **3**, 16670–16678.
48 C. Wang, K. Su, W. Wan, H. Guo, H. Zhou, J. Chen, X. Zhang and Y. Huang, *J. Mater. Chem. A*, 2014, **2**, 5018–5023.
49 G. Zhou, E. Paek, G. S. Hwang and A. Manthiram, *Nat. Commun.*, 2015, **6**, 7760.
50 J. Song, T. Xu, M. L. Gordin, P. Zhu, D. Lv, Y. B. Jiang, Y. Chen, Y. Duan and D. Wang, *Adv. Funct. Mater.*, 2014, **24**, 1243–1250.
51 M. Q. Zhao, X. F. Liu, Q. Zhang, G. L. Tian, J. Q. Huang, W. Zhu and F. Wei, *ACS Nano*, 2012, **6**, 10759–10769.
52 C. Tang, Q. Zhang, M. Q. Zhao, J. Q. Huang, X. B. Cheng, G. L. Tian, H. J. Peng and F. Wei, *Adv. Mater.*, 2014, **26**, 6100–6105.
53 Y. L. Ding, P. Kopold, K. Hahn, P. A. van Aken, J. Maier and Y. Yu, *Adv. Funct. Mater.*, 2016, **26**, 1112–1119.
54 J. Yang, J. Xie, X. Zhou, Y. Zou, J. Tang, S. Wang, F. Chen and L. Wang, *J. Phys. Chem. C*, 2014, **118**, 1800–1807.
55 W. Zhou, C. Wang, Q. Zhang, H. D. Abruña, Y. He, J. Wang, S. X. Mao and X. Xiao, *Adv. Energy Mater.*, 2015, **5**, 1401752.
56 H. Wang, Y. Yang, Y. Liang, G. Zheng, Y. Li, Y. Cui and H. Dai, *Energy Environ. Sci.*, 2012, **5**, 7931–7935.
57 S. A. Freunberger, Y. Chen, Z. Peng, J. M. Griffin, L. J. Hardwick, F. Bardé, P. Novák and P. G. Bruce, *J. Am. Chem. Soc.*, 2011, **133**, 8040–8047.
58 J. S. Lee, S. Tai Kim, R. Cao, N. S. Choi, M. Liu, K. T. Lee and J. Cho, *Adv. Energy Mater.*, 2011, **1**, 34–50.
59 S. Yang and H. Knickle, *J. Power Sources*, 2002, **112**, 162–173.
60 D. U. Lee, J. Y. Choi, K. Feng, H. W. Park and Z. Chen, *Adv. Energy Mater.*, 2014, **4**, 1301389.
61 F. Cheng and J. Chen, *Chem. Soc. Rev.*, 2012, **41**, 2172–2192.
62 J. Zhang, Z. Zhao, Z. Xia and L. Dai, *Nat. Nanotechnol.*, 2015, **10**, 444–452.
63 Z. Liu, H. Nie, Z. Yang, J. Zhang, Z. Jin, Y. Lu, Z. Xiao and S. Huang, *Nanoscale*, 2013, **5**, 3283–3288.
64 X. Zhou, Z. Bai, M. Wu, J. Qiao and Z. Chen, *J. Mater. Chem. A*, 2015, **3**, 3343–3350.
65 C. Zhao, C. Yu, S. Liu, J. Yang, X. Fan, H. Huang and J. Qiu, *Adv. Funct. Mater.*, 2015, **25**, 6913–6920.
66 E. Yoo, J. Nakamura and H. Zhou, *Energy Environ. Sci.*, 2012, **5**, 6928–6932.
67 K. Gong, F. Du, Z. Xia, M. Durstock and L. Dai, *Science*, 2009, **323**, 760–764.
68 R. Mi, S. Li, X. Liu, L. Liu, Y. Li, J. Mei, Y. Chen, H. Liu, H. Wang, H. Yan and W. M. Lau, *J. Mater. Chem. A*, 2014, **2**, 18746–18753.
69 S. Zhu, Z. Chen, B. Li, D. Higgins, H. Wang, H. Li and Z. Chen, *Electrochim. Acta*, 2011, **56**, 5080–5084.
70 H. W. Liang, Z. Y. Wu, L. F. Chen, C. Li and S. H. Yu, *Nano Energy*, 2015, **11**, 366–376.
71 J. Shui, F. Du, C. Xue, Q. Li and L. Dai, *ACS Nano*, 2014, **8**, 3015–3022.

72 G. Panomsuwan, S. Chiba, Y. Kaneko, N. Saito and T. Ishizaki, *J. Mater. Chem. A*, 2014, **2**, 18677–18686.
73 C. Shu, Y. Lin and D. Su, *J. Mater. Chem. A*, 2016, **4**, 2128–2136.
74 H. W. Liang, X. Zhuang, S. Brüller, X. Feng and K. Müllen, *Nat. Commun.*, 2014, **5**, 4973.
75 K. Zhang, L. Zhang, X. Chen, X. He, X. Wang, S. Dong, L. Gu, Z. Liu, C. Huang and G. Cui, *ACS Appl. Mater. Interfaces*, 2013, **5**, 3677–3682.
76 X. Guo, P. Liu, J. Han, Y. Ito, A. Hirata, T. Fujita and M. Chen, *Adv. Mater.*, 2015, **27**, 6137–6143.
77 H. W. Park, D. U. Lee, L. F. Nazar and Z. W. Chen, *J. Electrochem. Soc.*, 2013, **160**, A344–A350.
78 J. L. Shui, N. K. Karan, M. Balasubramanian, S. Y. Li and D. J. Liu, *J. Am. Chem. Soc.*, 2012, **134**, 16654–16661.
79 M. D. Slater, D. Kim, E. Lee and C. S. Johnson, *Adv. Funct. Mater.*, 2013, **23**, 947–958.
80 S. W. Kim, D. H. Seo, X. Ma, G. Ceder and K. Kang, *Adv. Energy Mater.*, 2012, **2**, 710–721.
81 N. Yabuuchi, K. Kubota, M. Dahbi and S. Komaba, *Chem. Rev.*, 2014, **114**, 11636–11682.
82 J. L. Liu, Z. Chen, W. Xuan, S. Chen, B. Zhang, J. Wang, H. Wang, B. Tian, M. Chen, X. Fan, Y. Huang, T. Sum, J. Lin and Z. X. Shen, *ACS Nano*, 2017, **11**, 6911–6920.
83 Y. Cao, L. Xiao, M. L. Sushko, W. Wang, B. Schwenzer, J. Xiao, Z. Nie, L. V. Saraf, Z. Yang and J. Liu, *Nano Lett.*, 2012, **12**, 3783–3787.
84 Y. X. Wang, S. L. Chou, H. K. Liu and S. X. Dou, *Carbon*, 2013, **57**, 202–208.
85 K. Tang, R. J. White, X. Mu, M. M. Titirici, P. A. van Aken and J. Maier, *ChemSusChem*, 2012, **5**, 400–403.
86 S. Wenzel, T. Hara, J. Janek and P. Adelhelm, *Energy Environ. Sci.*, 2011, **4**, 3342–3345.
87 J. Sun, H. W. Lee, M. Pasta, H. Yuan, G. Zheng, Y. Sun, Y. Li and Y. Cui, *Nat. Nanotechnol.*, 2015, **10**, 980–985.
88 J. Xu, M. Wang, N. P. Wickramaratne, M. Jaroniec, S. Dou and L. Dai, *Adv. Mater.*, 2015, **27**, 2042–2048.
89 S. Wang, L. Xia, L. Yu, L. Zhang, H. Wang and X. W. Lou, *Adv. Energy Mater.*, 2016, **6**, 1502217.
90 T. Yang, T. Qian, M. Wang, X. Shen, N. Xu, Z. Sun and C. Yan, *Adv. Mater.*, 2016, **28**, 539–545.
91 X. Xie, K. Kretschmer, J. Zhang, B. Sun, D. Su and G. Wang, *Nano Energy*, 2015, **13**, 208–217.
92 W. Li, S. Hu, X. Luo, Z. Li, X. Sun, M. Li, F. Liu and Y. Yu, *Adv. Mater.*, 2017, **29**, 1605820.
93 Y. Liu, N. Zhang, L. Jiao and J. Chen, *Adv. Mater.*, 2015, **27**, 6702–6707.
94 J. Gu, Z. Du, C. Zhang and S. Yang, *Adv. Energy Mater.*, 2016, **6**, 1600917.
95 G. Zhou, E. Paek, G. Wang and A. Manthiram, *Nat. Commun.*, 2015, **6**, 7760.